Science Telescope for Gravity Probe B

S. Wang[a], R. P. Farley[b], J. H. Goebel[c], M. Heifetz[a], J. A. Lipa[a] and J. P. Turneaure[a]

[a]Hansen Experimental Physics Laboratory, Stanford University, Stanford, California, U.S.A
[b]Lockheed-Martin Missiles and Space, Palo Alto, California, U.S.A.
[c]Space Projects Division, NASA Ames Research Center, Mountain View, California, U.S.A.

ABSTRACT

The Gravity Probe B Relativity Mission uses a fused-quartz optical star tracking telescope as the sensor for the control system which points the spacecraft towards its guide star. The telescope is cooled to < 5 K while the readout which uses photodiodes and JFET preamps operates at 72 K. It is mounted on the front end of the telescope with a thermal standoff. Analysis indicates that the telescope is capable of providing sub-milli-arc-second (marcs) pointing stability information with an angular pointing noise of < 21 marcs/$\sqrt{Hz}$ for the guide star IM Pegasi. We describe the design of the telescope and test results under nominal operating conditions. Analysis of the expected performance of the telescope in flight, based on the test results, is also presented.

Keywords: GP-B, Relativity Mission, optical telescope, fused quartz, low temperature, silicon JFET, star tracker

1. INTRODUCTION

The purpose of the Gravity Probe B (GP-B) Relativity Mission is to measure two effects in general relativity by using low drift gyroscopes. The main science objective of GP-B is to measure the so-called geodetic effect to 1 part in 10^4 and the associated frame dragging effect to 1%.[1] These phenomena are described in some detail in the book by Misner *et al.*[2] The London moment[3] generated by a spinning superconductor provides the basic mechanism for readout of the gyroscope spin axis. This magnetic moment is measured by readout loops, which provide information on the direction of the gyro spin axis. The change of the spin direction with time provides the relativity signal. To achieve a precision measurement of the gyro spin direction with respect to an inertial reference frame over a period of more than a year, a stable reference is provided by a star tracking telescope, which is referenced to the gyro readout loop by a rigid mechanical structure. The effects of long term drift in this structure are attenuated by rolling the spacecraft about the line of sight to the star.

In this paper, we describe the telescope hardware, its specifications and how they are related to the science objectives of the mission through test results and analysis.

2. HARDWARE DESCRIPTION

The main optical system of the telescope is a variation of the Cassegrain-Schmidt design with the addition of a tertiary mirror. The purpose of the tertiary mirror is to bring the image to the entrance pupil of the telescope, simplifying the construction of the readout optics. All optical components are made from fused quartz (Herasil 1-top) produced by Heraeus-Amersil*. The components were pre-cut by Speedring† and fine cut and polished by General Optics‡. The primary mirror was first cut to a concave spherical shape with a radius of curvature of 1.206 m. Unlike conventional Cassegrain-Schmidt telescopes with a corrector plate, the spherical aberration in our design is corrected by figuring the primary mirror with an aspheric correction. This figuring was done by Tucson Optical Research§. The secondary and tertiary mirrors are both spherical convex mirrors with radii of curvature of 2.317 m and 0.190 m, respectively. The selection of the curvature of the secondary and tertiary mirrors is such that a large effective focal length can be obtained with a small physical length allowing a mechanical design with a high structural strength. At the same time, the values of the radii of curvature are chosen to be within reach

*Heraeus Quarzglas GmbH & Co. KG, Quarzstrasse, D-63450 Hanau, Germany
†Speedring, Inc, 6767 Al Highway 157, Cullman, Alabama
‡General Optics, Inc., 554 Flinn Ave., Moorpark, California
§Tucson Optical Research Group, 210 S. Plumer Ave., Tucson, Arizona

Cryogenic Optical Systems and Instruments X, James B. Heaney, Lawrence G. Burriesci, Editors, Proceedings of SPIE Vol. 5172 (2003) © 2003 SPIE · 0277-786X/03/$15.00

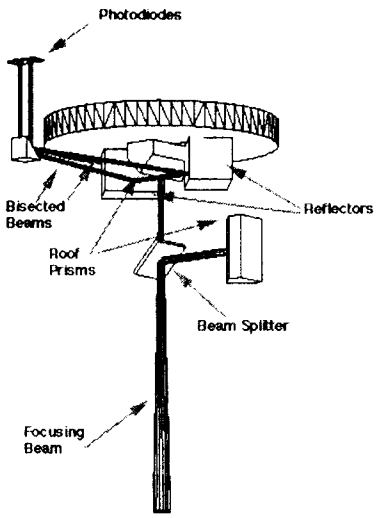

Figure 1. Light Path for the image divider and detectors.

of conventional fabrication processes while still meeting the accuracy requirements for the optical components. Instead of the usual corrector plate, an optically flat window called the forward plate is placed at the entrance to the telescope. Both the primary and tertiary mirrors are mounted on the base plate. The secondary mirror is mounted on the forward plate, which also supports the image processing components as well as thermometers. The base plate and the forward plate are joined via a simple tube with a nominal length of 0.349 m. The final length of this tube is adjusted until the focal point of the telescope is located 2.98 $\pm$ 0.05 cm above the forward plate. The adjustment of the tube length is a very slow process since the end surfaces need to be parallel within 1 arcs and a unit length change in the tube causes about 60 times the change in focal position. The final adjustment of the focal position is achieved by changing the thickness of a fused quartz shim placed between the image divider assembly and the forward plate. The clear aperture is defined by a narrow ring of aluminum mirror coating on the forward plate. The central obscuration is determined by a reticle mirror mounted on top of the forward plate and used both for testing the telescope and for coordinate transfer of the gyro readout loops to the spacecraft coordinate system.

Just prior to coming into focus, the optical beam passes through a beam splitter inside the image divider assembly mounted on the forward plate. The two beams fall onto roof prisms having very sharp edges at the focal point. The roof prisms are oriented so that they bisect the images in orthogonal directions. Each pair of bisected images is folded and fed through a pair of adjacent field lenses and relayed into a detector package assembly (DPA). The DPA has a focusing lens at its entrance. The pair of converging light beams passes through a second beam splitter and falls onto primary and redundant detectors respectively. Fig. 1 shows a schematic of the light path for one of the axes. For clarity, the lenses and beam splitters for the bisected beams are not shown. Also not shown are the beams crossing at the entrance of the DPA. The field lenses for the bisected beams are designed so that the image size on the photodiode is comparable with the sensor area. Also, the movement of the image on the photodiode sensor is such that the entire image remains on the sensor over the complete field of view of the telescope.

All the mirror coatings are enhanced aluminum films with a silicon dioxide overcoat. The typical reflection coefficient of these coatings at visible wavelengths is about 90%.

Fig. 2 shows the mechanical design of the telescope. The base plate was designed with a hollow tubular section as an extra precaution to minimize the cryogenic focal shift due to the potential mismatch of the coefficient of thermal expansion between the base and the gyroscope assembly.[4] All the fused quartz components were bonded together with either sodium hydroxide or potassium hydroxide,[5] ensuring a high mechanical strength and reliability.

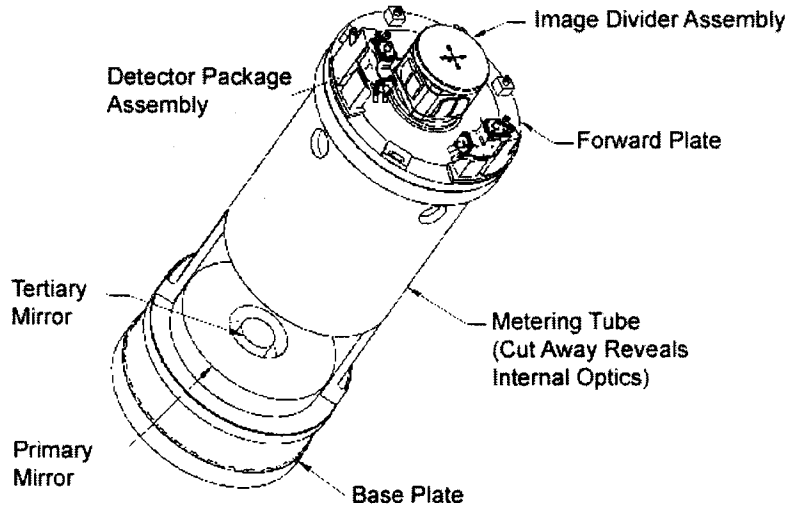

Figure 2. Telescope Assembly. The outside diameter of the telescope is 0.184 m and the overall length is about 0.48 m.

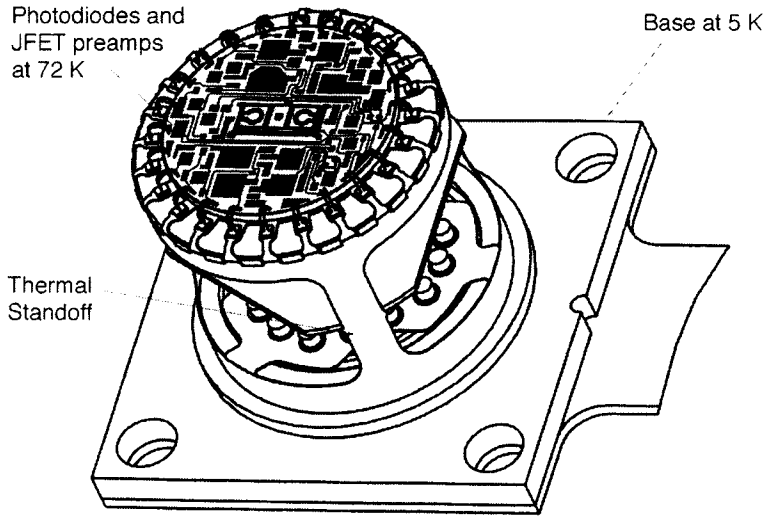

Figure 3. Telescope detector assembly. Not shown are the patterned conducting film electrical wires on the Kapton film support structure. The diameter of the sapphire platform is about 1.2 cm.

Each of the DPA's contains two detector assemblies comprising primary and redundant readouts. The detector assemblies contain a matched pair of blue-enhanced silicon photodiodes and silicon JFET amplifier circuits operating in a charge-locked loop mode to keep the potential across the photodiode at a constant reverse bias of about 4 V, optimizing the linearity. The photodiodes and JFET circuits are mounted on a sapphire thermal platform and maintained near 72 K for optimal noise performance.[6,7] Thermal isolation is achieved using a Kapton support structure with thin film electrical connections. Fig. 3 shows a diagram of the detector assembly. Fig. 4 shows the circuit diagram with the cold electronics to the left side of the vertical dashed line. The charge-locked loop is reset at a 10 Hz rate. At this reset rate, the voltage ramp due to the charge integrator reaches a reasonable value, well below saturation. At the same time, the charge reset frequency is high enough that the signal is not dominated by 1/f noise.

An important part of the optical system, which is not physically attached to the telescope, is a set of cryogenic

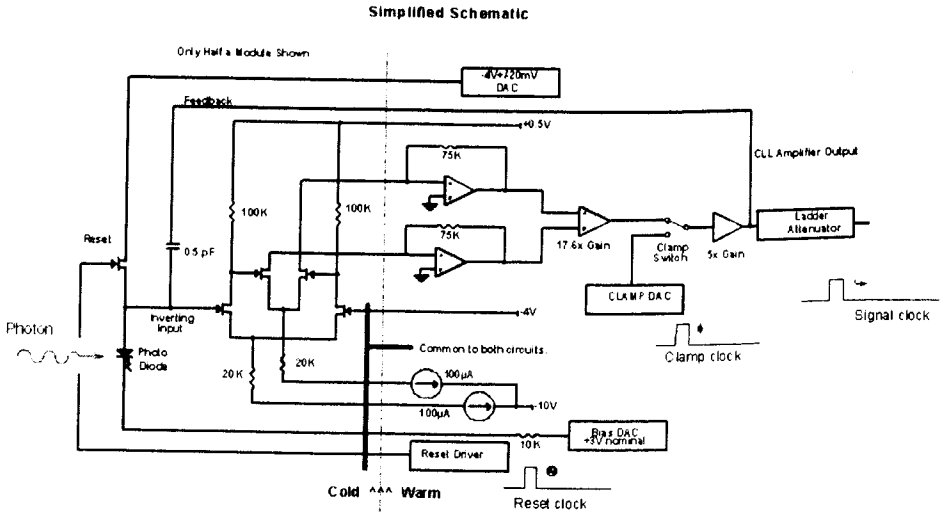

Figure 4. Simplified telescope readout circuit. The circuit shown is for one diode. A second identical circuit is mounted on the same sapphire substrate. The input points marked by the bold vertical line are common to both low temperature circuits receive signals from a single room temperature driving circuit to minimize the number of connector contacts in the assembly.

windows. The outer window, which serves as a vacuum seal for the gyroscope enclosure, is made of single crystal sapphire with its a-axis parallel to the optical axis. It has both an EMI shield and an anti-reflection coating on each side. For most of the visible optical band, the transmission coefficient of the coated window is higher than 80%. The three inner windows are made of Herasil 1-top fused quartz with anti-reflection coatings on both sides. During flight, the windows are expected to have operating temperatures of 238 K, 129 K, 72 K and 28 K. The fused quartz windows were tested for their wavefront quality in an assembly using the same relative orientations as in the final installation.[8] The wavefront quality of the coated sapphire window was measured only at room temperature. Its r.m.s. wavefront error was found to be $< 0.016\ \lambda$ at 633 nm. The wavefront quality of the flight window assembly in the spacecraft was indirectly measured during the payload test.[9,10]

3. TELESCOPE PERFORMANCE AND SPECIFICATIONS

In this section, we discuss the specifications and the performance of the telescope. Since the telescope is used only as a star tracker to provide the pointing information for the spacecraft, its emphasis on performance is different from that of conventional telescopes used for imaging. The primary requirements on the telescope are for high tracking sensitivity and pointing bias stability and low pointing noise.

The telescope response function for each detector can be expressed by:

$$R_+(\theta_x) = \frac{1}{N}\int_{\theta_x}^{\infty} d\theta_x \int_{-\infty}^{\infty} d\theta_y \int_0^{\infty} I(\theta,\lambda,\Phi)F(\theta)Q_+(\lambda)T_+(\lambda)P(\lambda)d\lambda \tag{1}$$

and

$$R_-(\theta_x) = \frac{1}{N}\int_{-\infty}^{\theta_x} d\theta_x \int_{-\infty}^{\infty} d\theta_y \int_0^{\infty} I(\theta,\lambda,\Phi)F(\theta)Q_-(\lambda)T_-(\lambda)P(\lambda)d\lambda \tag{2}$$

respectively where subscripts "+" and "-" indicate quantities for detectors on the positive and negative direction of the same axis, and θ_x and θ_y are incident angles along the x and y directions,

$$N = \int_{-\infty}^{\infty} d\theta_x \int_{-\infty}^{\infty} d\theta_y \int_0^{\infty} I(\theta,\lambda,\Phi)F(\theta)Q(\lambda)T(\lambda)P(\lambda)d\lambda \tag{3}$$

is the normalization factor, where $\theta = \sqrt{\theta_x^2 + \theta_y^2}$ is the light incident angle relative to the optical axis of the telescope, λ is the wavelength of the star light and Φ is the wavefront error of all the optical components up to the roof prism in units of λ_0, the measurement wavelength. $I(\theta, \lambda, \Phi)$ is the light intensity distribution function at the roof edge, $F(\theta)$ is the telescope field stop function, $Q(\lambda)$ is the quantum efficiency of the photodiodes, $T(\lambda)$ is the optical transmission coefficient from the entrance of the windows to the photodiode sensor, and $P(\lambda)$ is the guide star spectrum.

The tracking sensitivity is defined as

$$S_T = \frac{d(\Delta R)}{d\theta} \tag{4}$$

where

$$\Delta R = R_+ - R_- \tag{5}$$

For a ground test, we cannot simulate the star spectrum very effectively, therefore the response functions given in Eqs (1) and (2) cannot be measured directly. Since the star spectrum is part of the integrand, we need to measure or simulate each part of it to obtain an estimate of the actual response function.

The Strehl ratio is defined as the ratio of the peak intensity of the diffraction spot of a real optical system to the intensity of the Airy disk in a corresponding ideal system. For a random wavefront error of rms value Φ, the Strehl ratio is given by[11]

$$R_s \doteq e^{-(2\pi\Phi)^2} \tag{6}$$

For the telescope system including the windows, neither the Strehl ratio nor the intensity distribution function can be measured directly. Instead the response function as described by Eq. (1) is measured at a single wavelength near the center of the optical band. The analysis methodology we adopted was to assume that the wavefront error was equivalent to a focal error, to then calculate the response function for a given Strehl ratio, and to fit the calculation to the measurement. The intensity distribution function corresponding to that focal error was then used for the telescope system analysis. The advantage of this method is that the required intensity distribution functions can be obtained numerically from a formula given by Born and Wolf.[12]

Table 1 lists the final specifications related to the science telescope along with our present estimates. The specifications were derived so that the telescope would achieve the science objectives within the known constraints. In the subsequent sections, we discuss these items.

Table 1. Specifications for GP-B Science Telescope

PARAMETER	REQUIREMENT	ESTIMATE
Central Obscuration (m)	0.070	0.070
Clear Aperture (m)	0.144	0.144
Focal Length (m)	3.81	3.81
Field of View at 10% Peak Intensity (arcs)	> 60	> 66
Range of Monotonic Response (arcs)	> 1	> 1.9
Linear Bias Drift (marcs/yr)	< 0.1	< 0.058
Perpendicularity of Readout Axes (degree)	< 1	0.4 ± 0.2
Optical Transmission	$> 10\%$ (400 nm - 1000 nm)	$> 13\%$
Tracking Sensitivity (1/arcs)	$1.4 \geq d\Delta R/d\theta \geq 0.4$	$1.27 \geq d\Delta R/d\theta \geq 0.44$
Pointing Noise (marcs/$\sqrt{Hz}$ @ 10 Hz)	≤ 100	< 21

3.1. Clear Aperture

The clear aperture is chosen so that the first minimum of the Airy disk is about 1 arcs from the center of the image. For such an Airy disk size, we will be able to resolve about 0.1 marcs if the noise is at the level of 0.01 % of the maximum signal. This is conveniently achievable in most of the test setups with signal averaging. At the same time it allows enough dynamic range for the tracking system. Other concerns for the clear aperture selection include keeping the thermal radiation low and keeping the entering light energy high. For a clear aperture of 0.144 m diameter, the black body radiation power at 300 K is about 7 W. The cryogenic windows block most of the thermal radiation and the actual radiation power reaching the instrument is about 10 μW which is negligible compared with other heat leaks. In section 3.7, we will see that this aperture provides enough transmission of visible light to meet the tracking noise requirement.

3.2. Focal Length

The focal length determines the linear dimension of the diffraction limited image size. For our selection of the aperture and focal length, the image size is about 30 μm in diameter. This image size can be accurately divided by a high quality roof prism.

3.3. Field of View at 10% Peak Signal

The telescope needs to have a wide enough field so that during the initial star acquisition phase, it will take relatively short time to find the guide star. With a one arc-minute (arcm) field of view, for a initial scan range of 1 $\times$ 1 degree, it will take 3600 scan points to do the scan in a few hours, which is reasonable compared to the mission duration. The aperture stop sets the full intensity aperture to about 43 arcs. Since the stop is located in the primary converging beam, the signal on the detector does not drop sharply when the incident light moves out of the field of view. Instead, near the field edge, the detector sees a gradual change in signal over about 30 arcs. The net field of view to the 10% intensity level is then 66 arcs.

3.4. Range of Monotonic Response

This specification can be interpreted in terms of the quality of the sharpness of the roof prism edges and the uniformity in reflectivity of the associated coatings. It assures that the spacecraft pointing control receives an unambiguous signal when the pointing drifts away from the guide star. Crossing into this range from the outside, the control system transitions from a slew-rate control to a proportional-integral-differential control. This range is measured by inspecting the tracking sensitivity data and finding the range in which the tracking sensitivity does not have a sign change within the measurement error.

3.5. Linear Bias Drift

With a non-rolling spacecraft, the linearity bias drift can mimic the science signal. Therefore, it must be consistent with the GP-B science objective of 0.1 marcs/yr.[1] measurement accuracy. With a rolling spacecraft, the main issue is the introduction of angle bias at the roll frequency due to any non-linearity. The rolling of the spacecraft is an important concept that eliminates the body-fixed biases from the science signal. In effect, any signal which is not at the roll rate is filtered out from the science signal.

3.6. Perpendicularity between Readout Axes

This requirement is needed to limit the cross-correlation between nominally orthogonal readout axes. The one degree requirement limits the cross-correlation to about 1% level. The impact of this on the science signal is that when the roll axis of the spacecraft is not exactly on the optical axis, the angle between the two needs to be calculated based on the orientations of the readout axes. A lack of perpendicularity between the telescope readout axes would introduce bias into such a calculation. But since the roll axis is controlled to be within 100 marcs of the optical axis, such corrections are typically small. The perpendicularity is measured by checking cross-coupling between orthogonal readout outputs with respect to orthogonal incident light scans.

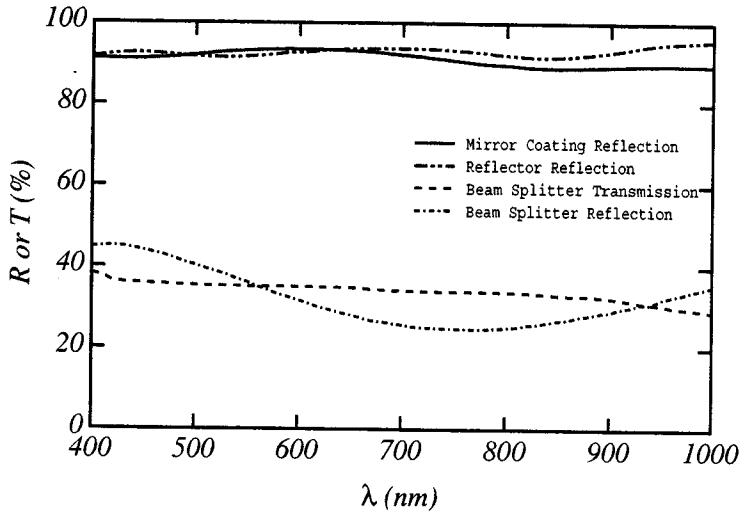

Figure 5. Optical transmission or reflection coefficients for typical samples used for telescope components as a function of wavelength.

3.7. Optical Transmission

The optical transmission is specified over the Si photodiode operating bandwidth of 400 nm to 1000 nm. The optical transmission, the Strehl ratio, the quantum efficiency and the readout noise combine to determine the tracking sensitivity as shown in Eq. (4).

The transmission is measured at a single wavelength for the optical system. The spectral response of the system is assumed to be the same as observed at room temperature. The spectral response which needs to be considered includes the transmission through the fused quartz and sapphire windows, the transmission through the window coatings, the reflections from the mirror coatings and the reflection and transmission from the beam splitter coatings. Fig. 5 shows these spectral responses from typical samples fabricated at the same time as the flight parts.

3.8. Quantum Efficiency

The spectral response of the blue-enhanced photodiodes was provided by the vendor (Centronic Ltd[¶]). The cryogenic response was assumed to be the same as that at room temperature in the present analysis. It was recently found that there might be a drop in quantum efficiency above 800 nm at low temperatures. This is currently under investigation. Fig. 6 shows the quantum efficiency as a function of the wavelength. The symbols represent data provided by the vendor and the line is a Legendre polynomial fit to the data.

3.9. Star Spectrum

The baseline guide star for GP-B is IM Pegasi (HR 8703). Its optical and near infrared spectra were measured[13] with the FAST spectrograph on the Mt. Hopkins 1.5 m telescope. Fig. 7 shows the resulting spectral irradiance of the star. Since the measurement was performed on a ground-based telescope, various atmospheric infrared absorption bands exist in the data. For our analysis, a Lengendre polynomial fit to the data was used.

3.10. End-to-end Responsivity

Due to variations in the optical coatings, especially in the beam splitters, the end-to-end responsivity for the 8 detectors span a wide range. Table 2 lists the end-to-end responsivity for each detector at a wavelength of 668 nm. The responsivity values are for the off axis but full transmission situation (for incident angles in the range of 4 to 30 arcs). At null pointing, these values are nominally 1/2 of those listed.

[¶]Centronic Ltd, Centronic House, King Henry's Drive, New Addington, Surrey, U.K.

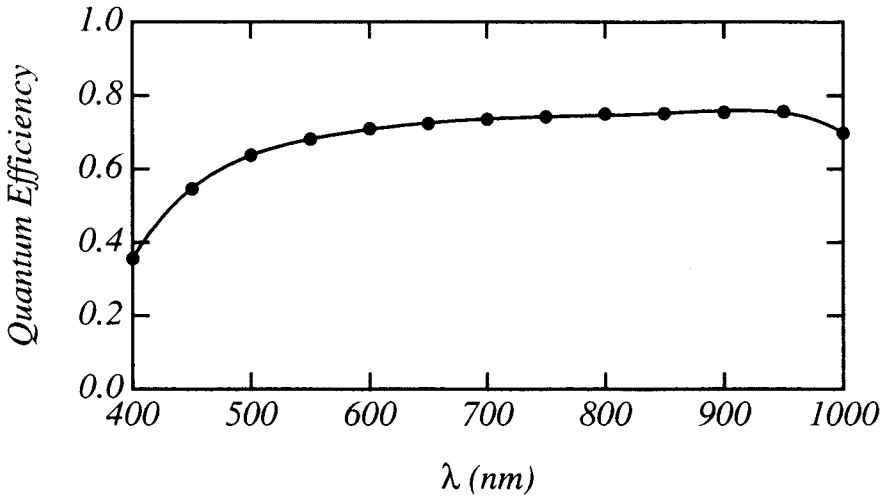

Figure 6. Quantum efficiency of the blue-enhanced photodiodes.

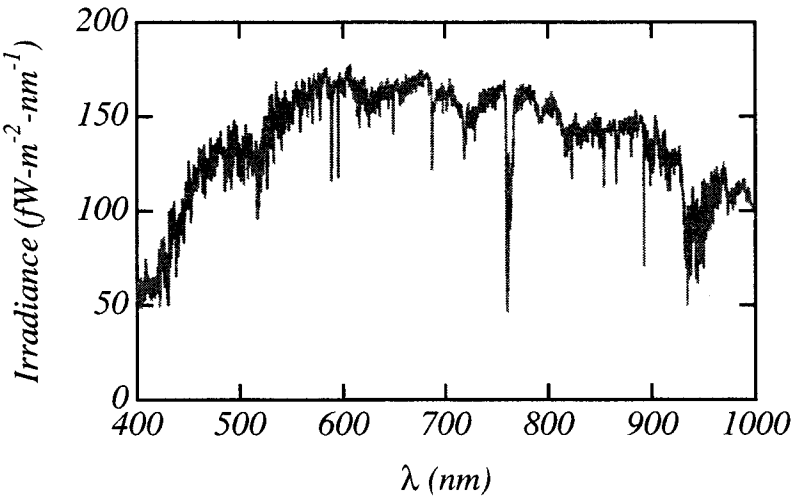

Figure 7. Irradiance of IM Pegasi (HR 8703).

Table 2. End-to-end responsivity for each detector at 668 nm

Detector	Responsivity (mA/W)
1	8.41
2	8.44
3	22.71
4	20.54
5	12.88
6	12.68
7	12.14
8	10.60

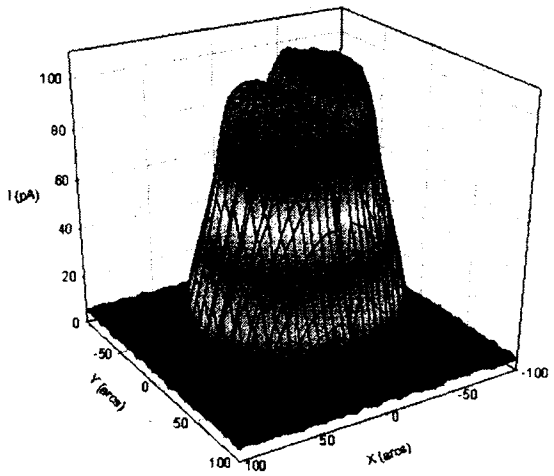

Figure 8. Telescope detector output vs. pointing angle. A monochromatic light of wavelength 685 nm is used for the test.

4. TEST AND ANALYSIS RESULTS

The telescope both as a subsystem and when integrated into the payload was tested with artificial star facilities. In both artificial star facilities (AS#2 and AS#3), the light source was the output of an optical fiber coupled to a laser diode of single wavelength. The wavelength used for AS#2 was 685 nm while for AS#3 it was 668 nm. Fig. 8 shows the detector response as a function of pointing angle for one pair of detectors. For this measurement, the incident angle is raster scanned over a 200 $\times$ 200 arcs range centered around the optical axis. The data displayed are the output from a pair of detectors sensitive to the x-axis motion of the star image. When the light beam is scanned from negative side of the x-axis to the positive side, the image goes from one side of the corresponding roof prism to the other side and therefore the light changes from the detector on the negative side to the detector on the positive side. From this measurement, we can easily obtain the field stop function $F(\theta)$ as defined in Eq. (1). The differences in the height of the signals from the two channels is most likely due to the differences in the transmission and reflection coefficients along the optical paths of the two beams after bisection at the roof prism.

4.1. Tracking Sensitivity

From information similar to that described in the previous sections, the tracking sensitivity, S_T, of the telescope on orbit was calculated to be between 0.44 to 1.27 per arcs using an end-to-end model of the optics. The lower value was obtained by assuming a most conservative estimate of the errors which degrade the tracking sensitivity. The largest error included was the uncertainty in the on-orbit focal position due to thermal effects on the windows. The upper value corresponds to an estimate for a telescope and windows system with diffraction limited optics.

4.2. Pointing Noise

Since the amplifier noise exceeds the photon noise in the telescope readout system, the pointing noise can be directly measured by blocking all light entering the telescope. Based on the payload test results, the estimated pointing noise is < 21 marcs/$\sqrt{Hz}$.

4.3. Linear Bias Drift

The linear bias drift was calculated based on an end-to-end analysis of the entire system, including the effects of variations of material properties and environmental conditions on the optical and electronic performance of all the subsystems. A ^{TM}Mathematica model was set up for this calculation. In the model, the optical and electronic properties were based on test results while the material properties were based on the published literature or conservative estimates. The estimated linear bias drift is such that its effect on the science signal is < 0.058 marcs/yr.

5. SUMMARY

The science telescope for Gravity Probe B has been tested in various phases of the integration prior to launch. It was tested as a subsystem in the AS#2 facility, and then tested at the payload level with the AS#3 facility. Recently it was retested for electronic noise using the flight telemetry system. For the guide star IM Pegasi, the expected tracking sensitivity of the telescope is 0.44/arcs at worst and 1.27/arcs at best, the pointing noise is estimated to be < 21 marcs/$\sqrt{Hz}$ and the estimated linear bias drift effect is < 0.058 marcs/yr.

ACKNOWLEDGMENTS

The development of the GP-B science telescope has involved the effort of many individuals. Here we have attempted to acknowledge those individuals who made contributions to the telescope development. Undoubtedly such an effort might not be as thorough as we wish, and some individuals might be inadvertently left out in this list. To those individuals, we offer our sincere apologies.

We would like to acknowledge the pioneering conceptual work of Francis Everitt. Donald Davidson was instrumental in every phase of the telescope development. He designed the optics of the flight telescope as well as that of two prototype telescopes. He also designed artificial stars #1 and #2 for room temperature and cryogenic testing of the telescope system. We extend our deep appreciation to Jason Gwo for his heroic effort in testing telescope #1 at room temperature, his development of a new bonding technique for assembly of the telescope's glass components, his work on AS#2 and his effort in assembly of the flight and backup telescopes. We are grateful to Paul Schweiger for his work on optical components while at Davidson Optronics and for his work on developing the cryogenic windows while at Lockheed Martin. We are indebted to Randall Kirschman, M. Jhabvala, S. Babu and N. Das for their work in developing the cryogenic readout system. We thank Dan DeBra, Ted Acworth and Robert Bernier and other members of the AS#3 team for their development of the instrument and for payload testing and Aldo Rossi for help with its fabrication. We appreciate the efforts of Lynn Huff, Ken Triebes and Thomas Pope of Lockheed Martin in design and testing of the optical system. Paul Ehrensberger, Richard Wolcott and Howard Demroff played key roles in telescope electronics fabrication. Mark Sullivan and Enrique Romero were key players in design of detector package mechanical assembly as well as other design tasks. We thank Joe Hayden of Speedring and John Tardif of General Optics for their work on the optical fabrication. We thank Larry Sokolsky of Lockheed Martin for performing the thermo-mechanical structural analysis of the telescope. We thank Ken Bower for his support in telescope assembly as well as numerous other

technical support activities. We also wish to thank the following individuals for contributions in various stages of the telescope development: Duncan Davidson for manufacturing artificial stars #1 and #2. Wolfgang Jung, Karlheinz Merkle, Matthew Chuck, John Kirk, Daniel Semides, Mehmet Solyali, Frans Alkemade, Bruno Richet, Jay Anastas, Paul Limtiaco, Jeff Grant, Matthew Bye and Frank Chilese for mechanical systems, Dick Gummer of Precison Cryogenics for cryogenic systems, Richard van Patten, Roger Cliff, Keneth Coleman, Hao Shi, Peter Milford for electronics, Mark Tapley, Jeremy Kasdin, Fred Berkowitz and Ben Lange for system engineering and Kristopher Cumbermack and Daemon Clark for data analysis and window testing.

REFERENCES

1. C. W. F. Everitt, S. Buchman, D. B. DeBra, G. Keiser, J. M. Lockhart, B. Muhlfelder, B. W. Parkinson, and J. Turneaure, "Gravity Probe B: Countdown to launch," in *Gyros, Clocks, Interferometers ....: Testing Relativistic Gravity in Space*, C. Lammerzahl, C. W. F. Everitt, and F. Hehl, eds., pp. 52 – 82, Springer, Berlin, 2001.
2. C. W. Misner, K. Thorne, and J. Wheeler, *Gravitation*, W. H. Freeman and Co., 1973.
3. Y. Xiao, W. Felson, and C. H. Wu, "Observations of the london moment and trapped flux in precision gyroscopes," *IEEE Transactions on Applied Superconductivity* **3(1)**, p. 2144, 1993.
4. S. Wang, D.-H. Gwo, K. A. Bower, L. W. Huff, and J. A. Lipa, "Status of the cryogenic telescope and guide star for Gravity Probe B," *Adv. Space Res.* **25**, p. 1189, 2000.
5. D.-H. Gwo, "Ultra precision and reliable bonding method," *U.S. Patent #6,284,085* , 2001.
6. S. Wang, D.-H. Gwo, K. Bower, L. Huff, R. Kirschman, J. Lipa, M. Jhabvala, S. Babu, and N. Das, "Testing the GP-B telescope readout electronics on a flight quality telescope," *J. Phys. IV France* **8**, pp. Pr3–181, 1998.
7. H. Demoroff, S. Babu, M. Bye, K. Coleman, N. Das, D. B. DeBra, P. E. Jr., R. P. Farley, D. K. Gill, J. H. Goebel, M. Jhabvala, A. Kashani, E. Romero, and M. T. Sullivan, "The telescope readout electronics for the Gravity Probe B satellite," *J. Phys. IV France* **8**, pp. Pr3–175, 1998.
8. S. Wang, E. B. Acworth, R. J. Bernier, D. A. Clark, K. M. Cumbermack, P. F. Schweiger, and J. A. Lipa, "Optical performance of the star tracking telescope for Gravity Probe B," *Adv. Space Res.* **To be published**, COSPAR 33 Conference Proceedings.
9. E. B. Acworth, "An artificial star for in-situ telescope calibration," *Ph.D. Dissertation,* **Stanford University**, 2000.
10. R. J. Bernier, "Design, optics, controls and calibration of artificial star #3 for Gravity Probe B," *Ph.D. Dissertation,* **Stanford University**, 2000.
11. E. L. O'Neill, *Introduction to Statistical Optics, pp. 99 - 101*, Addison-Wesley, Reading, Palo Alto, London, 1963.
12. M. Born and E. Wolf, *Principles of Optics, 6th Ed., pg. 439, eq. (21)*, Pergamon Press, Oxford, New York, Toronto, Sydney, Frankfurt, 1986.
13. M. Ratner, "Report of measurements made by Nelson Caldwell at SAO, Whipple Observatory," *Private Communication* , 1997.